Fast Transient Boundary Control and Steady-State Operation of the Dual Active Bridge Converter Using the Natural Switching Surface

Germán G. Oggier, *Member, IEEE*, Martin Ordonez, *Member, IEEE*, Juan M. Galvez, *Student Member, IEEE*, and Federico Luchino, *Student Member, IEEE*

***Abstract*—This paper presents a boundary control scheme for dual active bridge (DAB) converters using the natural switching surface (NSS). The implementation of a curved switching surface for DAB converters is a new area of research undertaken in this paper. The proposed technique brings the benefit of unprecedented dynamic performance, already developed for nonisolated topologies (e.g., buck and boost), to this more complex isolated topology. The analysis provides insight into the natural trajectories of the DAB converters and creates an accurate framework in the normalized geometrical domain. As a result, the physical limits of the converter under study become evident. Those physical limits are exploited by employing the NSS to obtain fast transient response under start-up, sudden load transients, and reference change. In addition, fixed-frequency operation is one of the key features of the proposed control scheme, which allows optimizing the design of the high-frequency transformer. Experimental results are presented to validate the NSS for DAB converters and illustrate the benefits of the normalization technique.**

***Index Terms*—Boundary control, dc–dc isolated converters, dual active bridge (DAB) converter, natural switching surface (NSS).**

I. Introduction

BIDIRECTIONAL buck and boost dc–dc converters play an important role in the implementation of power electronics interfaces for future power systems such as hybrid wind/PV power generation [1] and hybrid electric vehicles [2]. For these applications the dual active bridge (DAB) converter is a suitable alternative since high efficiency and high power density can be obtained [3]–[5]. Since the DAB converter employs a high-frequency transformer connected to an active bridge at each side, it can provide a high voltage conversion ratio and galvanic isolation with bidirectional power flow [6]–[9]. Furthermore, as the DAB converter allows buck and boost operating modes, it is particularly suitable to be used as an interface of energy storage systems, like batteries and ultracapacitors, where the voltage fluctuates according to the state of charge [10], [11].

These applications require an optimum and robust dynamic response of the converter. Much research effort has been spent on new control methods to enhance the dynamic and static responses. Work reported in the literature have studied the dynamics of converters by using well-known small-signal modeling [12], [13], linear feedback controllers [14], and linear digital control [15]. These works assume a small signal excitation around a steady-state value in order to reduce the exact nonlinear large-signal model to a linear small-signal model. The design procedure using state feedback controllers (pole placement) presents some advantages in terms of simplicity and steady-state performance [16]. Furthermore, if a DSP is used to implement the control law, a discrete-time state-space model of the converter can be used in order to obtain a more precise model instead of a continuous one. However, since these techniques assume a small-signal excitation, important large signal dynamic effects are lost in this process with its associated control performance loss.

A harmonic modeling strategy to create a linearized dynamic model of a DAB converter and a feedforward compensation strategy is presented in [17]. This strategy allows improving the DAB converter transient response for load changes.

A nonlinear control law applied to the DAB converter by using feedback linearization techniques was recently proposed [18]. The control strategy is based on a simplified converter model that provides acceptable accuracy for frequencies an order of magnitude lower than the switching frequency. Thus, reference tracking is good enough in presence of load disturbances. Since only input and output voltages are used for the control scheme presented in [18], opportunities to increase the dynamic performance can be achieved by adding transformer current measurements.

According to previous discussion, advanced control techniques applied to the DAB converter is still a topic that has not been treated by the research community to obtain high closed loop performance. The use of transient performance enhancing solutions for DAB converters, such as nonlinear boundary control, is an emerging field of research that brings benefits to the DAB topology. In this paper, a nonlinear control law for the DAB converter is proposed by employing curved switching surfaces (SSs), a new innovation in the area of control for

Manuscript received September 23, 2012; revised November 24, 2012; January 21, 2013; accepted March 18, 2013. Date of current version August 20, 2013. Recommended for publication by Associate Editor D. Maksimovic.

G. G. Oggier is with the CONICET, and also with the Grupo de Electrónica Aplicada, Facultad de Ingeniería, Universidad Nacional de Río Cuarto, X5804BYA Río Cuarto, Argentina (e-mail: goggier@ieee.org).

M. Ordonez and J. M. Galvez are with the Department of Electrical and Computer Engineering, University of British Columbia, Vancouver, BC V6T 1Z4 Canada (e-mail: mordonez@ieee.org; jgalvez@ieee.org).

F. Luchino is with the School of Engineering Science, Simon Fraser University, Metro Vancouver, BC V6T 1Z4 Canada (e-mail: fluchino@ieee.org).

Color versions of one or more of the figures in this paper are available online at http://ieeexplore.ieee.org.

Digital Object Identifier 10.1109/TPEL.2013.2256150

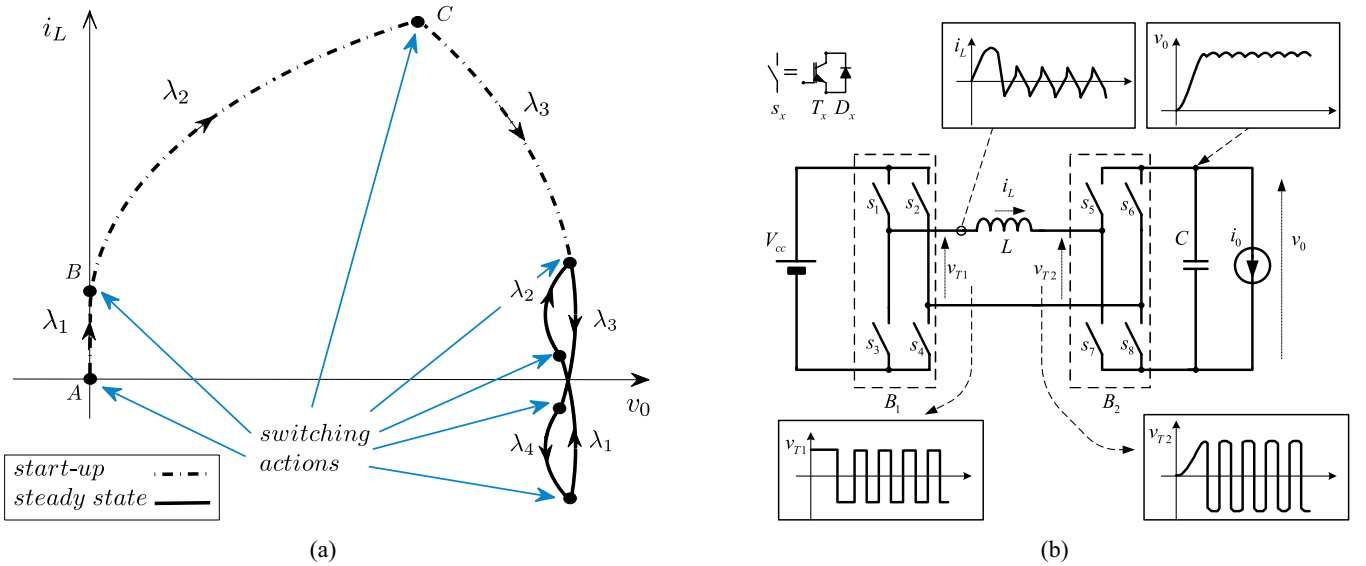

Fig. 1. (a) Phase plane showing conceptual trajectories when the NSS is used during start-up and steady-state operation and (b) Simplified scheme of the DAB converter showing the time domain voltage and current waveforms corresponding to the case shown in the phase plane.

isolated soft-switching topologies. By using SSs the dynamic response of the converter can be greatly improved with respect to the performance obtained by using small-signal linear controllers. The study of natural switching surfaces (NSS), which are based on the trajectories that follow the natural behavior of the converter has gained attention recently in the control of basic nonisolated topologies, like buck and boost converters, and voltage source inverters [19]–[21]. As well, a technique based on optimal trajectories for resonant converters was developed recently [22].

The objective of the investigations in this paper is to obtain an effective NSS control law with improved dynamic performance for a complex isolated topology—the DAB converter. This is illustrated conceptually in Fig. 1(a) during start-up operation. Fig. 1(b) shows a simplified schematic of the DAB converter, along with the voltage and current waveforms corresponding to the case shown in the phase plane of Fig. 1(a). The SSs are chosen in order to reach the steady-state condition with fast response. In steady-state operation, once the target operating point is reached, the control law ensures a switching sequence to prevent saturation of the high-frequency transformer. Both the output voltage and the transformer current are considered as varying references to establish a more accurate control law with excellent performance. As a result of the analysis, a control law for DAB converters defined as the DAB NSS is proposed.

The derivations are developed in the normalized domain to provide insight into the behavior of the DAB converter, leading to a geometrical treatment that is general and applicable to any possible set of specifications for DAB converters. The result of the analysis yields the NSS for DAB converters, featuring the ability to handle fast start-up transients, track changes of output voltage reference, and overcome load transients with unprecedented dynamic response. In addition to the enhanced dynamic response, fixed-frequency operation is one of the key features of the proposed control scheme, which allows optimizing the design of the high-frequency transformer and controlling the volt-second magnetizing balance to avoid saturation. An example is presented to illustrate characteristic features and the superior performance of the NSS, which are confirmed with simulation and experimental results of a 625 W DAB converter.

II. Dual Active Bridge (DAB) Converter

A simplified circuit schematic of a DAB topology is shown in Fig. 1(b) and it consists of a full bridge working as a dc–ac converter feeding a high-frequency transformer, which is connected to a second full bridge working as an ac–dc converter. The analysis of the DAB converter is simplified by reflecting the model to one side of the transformer and considering the transformer magnetizing inductance much larger than the leakage inductance. The DAB converter is, therefore, represented by two active full bridges linked by the transformer leakage inductance L. For the present analysis, the transformers turns ratio will be considered hereinafter equal to 1.

Fig. 2 shows the four different structures according to the state of the power switches, where solid lines correspond to active switches and dashed lines correspond to passive switches. Since the inductor current, i_L, can be positive or negative, the power transistor and diode of each switch are shown with a solid line. The different structures are defined as structure I when $v_L = V_{cc} + v_0$, structure II when $v_L = V_{cc} - v_0$, structure III when $v_L = -V_{cc} - v_0$, and structure IV when $v_L = -V_{cc} + v_0$. The power flow is controlled by switching both active bridges.

A constant output current loading condition is employed for the analysis due to its infinite impedance to represent both a large loading condition and the absence of damping effect—the worst case scenario in terms of stability. Simulation and experimental results are presented in Section VI in order to validate the analysis where fast transient is achieved for both constant output current and any other resistive loading condition.

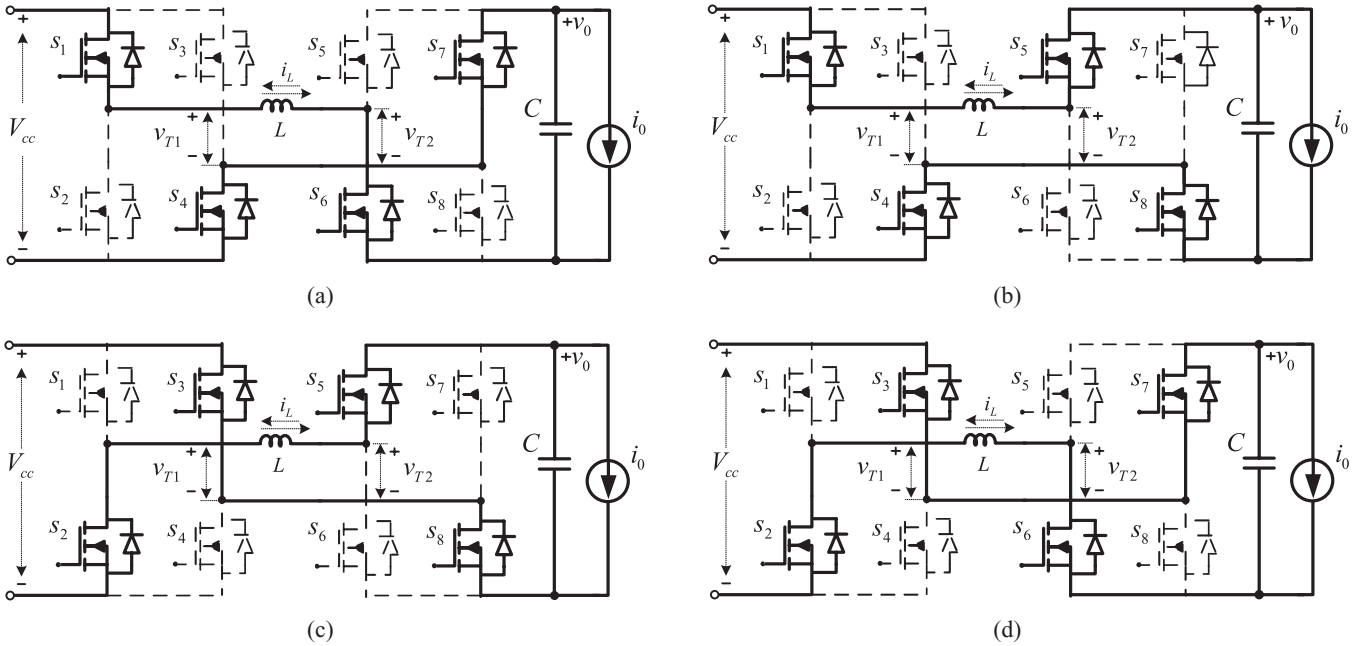

Fig. 2. DAB converter structures: (a) $v_L = V_{cc} + v_0$, Structure I; (b) $v_L = V_{cc} - v_0$, Structure II; (c) $v_L = -V_{cc} - v_0$, Structure III; (d) $v_L = -V_{cc} + v_0$, Structure IV.

III. Normalized Derivation for the DAB Converter

In this section, the normalization of the DAB converter is performed using the simplified schematic shown in Fig. 1(b). A normalized derivation is presented to provide generality and cover any possible combination of parameters: inductor value (L), output capacitor value (C), input voltage (V_{cc}), output power (P_0), and output voltage (V_0).

The derivation of the natural trajectories of the converter is presented to cover the different structures of the converter. The converter is modeled by a system of differential equations including the output voltage v_0 and inductor current i_L state variables as follows:

$$\frac{dv_0}{dt} = \frac{1}{C}\left(i_L u_2 - i_0\right) \tag{1}$$

$$\frac{di_L}{dt} = \frac{1}{L}\left(V_{cc} u_1 - v_0 u_2\right) \tag{2}$$

where $u_1 = 1$ and $u_1 = -1$ for $v_{T1} = V_{cc}$ and $v_{T1} = -V_{cc}$, respectively; and by $u_2 = 1$ and $u_2 = -1$ for $v_{T2} = v_0$ and $v_{T2} = -v_0$, respectively.

As shown in Fig. 2, the voltage applied to the leakage inductance can take four active levels: $(V_{cc} + v_0)$, $(V_{cc} - v_0)$, $(-V_{cc} - v_0)$, and $(-V_{cc} + v_0)$; depending on the state of the power switches.

The normalization is performed by using the characteristic impedance of the combined L and C values, $Z_0 = \sqrt{L/C}$, its natural frequency, $f_0 = 1/T_0 = 1/(2\pi\sqrt{LC})$, and the output voltage reference, V_r, as base quantities

$$v_{xn} = \frac{v_x}{V_r} \tag{3}$$

$$i_{xn} = \frac{i_x}{V_r} Z_0 \tag{4}$$

$$t_n = t.f_0 \tag{5}$$

where v_x and i_x represent generic voltages and currents, and v_{xn} and i_{xn} their respective normalized values. After performing the normalization, (1) and (2) can be rewritten as

$$\frac{dv_{0n}}{dt_n} = 2\pi\left(i_{Ln} u_2 - i_{0n}\right) \tag{6}$$

$$\frac{di_{Ln}}{dt_n} = 2\pi\left(V_{ccn} u_1 - v_{0n} u_2\right). \tag{7}$$

By combining (6) and (7), a general second-order differential equation can be obtained

$$\frac{d^2 i_{Ln}}{dt_n^2} = 4\pi^2 u_2\left(i_{0n} - i_{Ln} u_2\right). \tag{8}$$

The solution of this second-order system can be written as

$$i_{Ln} = A\cos\left(\beta t_n\right) + B\sin\left(\beta t_n\right) + i_{0n} u_2 \tag{9}$$

where $A = \left(i_{Ln}(0) - i_{0n} u_2\right)$, $B = \left(di_{Ln}(0)/dt_n\right)/\beta$ and $\beta = 2\pi$.

At the target operating point $v_{on} = V_{rn}$ where

$$V_{rn} = 1$$

and $i_{Ln}(0) = i_{Ln,\text{target}}$ is derived in order to operate the converter under constant switching frequency. Finally

$$\frac{di_{Ln}(0)}{dt_n} = 2\pi\left(V_{ccn} u_1 - V_{rn} u_2\right) = 2\pi\left(V_{ccn} u_1 - u_2\right). \tag{10}$$

By using the following trigonometric identity

$$A\cos x + B\sin x = \sqrt{A^2 + B^2}\sin\left[x + \tan^{-1}\left(\frac{A}{B}\right)\right] \tag{11}$$

the normalized inductor current, (9), can be rearranged as

$$i_{Ln} = \sqrt{A^2 + B^2}\sin\left[\beta t_n + \tan^{-1}\left(\frac{A}{B}\right)\right] + i_{0n}u_2. \quad (12)$$

By differentiating the normalized inductor current (12), the following expression can be obtained:

$$\frac{di_{Ln}}{dt_n} = 2\pi\left(V_{ccn}u_1 - v_{on}u_2\right) = \sqrt{A^2 + B^2}\,\beta\cos\left[\beta t_n + \tan^{-1}\left(\frac{A}{B}\right)\right]. \quad (13)$$

By isolating the argument of the trigonometric function in (12) and replacing in (13) the normalized time t_n can be eliminated given the following expression:

$$\frac{di_{Ln}}{dt_n} = \sqrt{A^2 + B^2}\beta\cos\left[\sin^{-1}\left(\frac{i_{Ln} - i_{on}\ u_2}{\sqrt{A^2 + B^2}}\right)\right] \quad (14)$$

and by using $\cos\left[\sin^{-1}(x)\right] = \sqrt{1 - x^2}$, (14) can be expressed as

$$\frac{di_{Ln}}{dt_n} = \left(\sqrt{A^2 + B^2}\right)\left(\sqrt{1 - \frac{\left(i_{Ln} - i_{on}\ u_2\right)^2}{\left(A^2 + B^2\right)}}\right). \quad (15)$$

After replacing $A = (i_{Ln,\text{target}} - i_{on}u_2)$ and $B = (V_{ccn}u_1 - u_2)$, the natural trajectories of the converter corresponding to the different operating modes can be expressed as

$$\lambda_{1,2,3,4} = \left(V_{ccn}u_1 - v_{0n}u_2\right)^2 - \left(i_{Ln,\text{target}} - i_{0n}u_2\right)^2 - \left(V_{ccn}u_1 - u_2\right)^2 + \left(i_{Ln} - i_{0n}u_2\right)^2. \quad (16)$$

where the subscripts correspond to natural trajectories for each of the structures depicted in Fig. 2.

These trajectories can be written in the following form:

$$(x - x_0)^2 + (y - y_0)^2 = r^2 \quad (17)$$

where $r = \sqrt{(i_{Ln,\text{target}} - i_{0n}u_2)^2 + (V_{ccn}u_1 - u_2)^2}$, $x = v_{0n}(-u_2)$, $x_0 = V_{ccn}u_1$, $y = i_{Ln}$, and $y_0 = i_{0n}u_2$.

The natural trajectories of the converter for the different modes are circles on the plane that shows the normalized inductor current versus the normalized output voltage of the converter. Fig. 3 shows the plane of the normalized inductor current versus the normalized output voltage, for buck and boost operating modes.

It should be noted that for constant output voltage reference and load current, the radius of each natural trajectory is a function of the initial conditions. Fig. 4 shows the evolution of the normalized output voltage and normalized inductor current for different initial conditions marked as A_x and B_x, for both operating modes. For example, analyzing the initial condition A in Fig. 4(a), two possible solutions can be used to reach the target:

1) Turn ON the power switches S_1, S_4, S_5, and S_8 in order to get the structure II (see Fig. 2) while $\lambda_3 < 0$. Thus, variables evolve according to natural trajectory λ_2 (dash-dot lines) with a radius established by the difference between the center of the circle corresponding to natural trajectory λ_2 and the point A. Once λ_3 becomes positive, then turn ON the corresponding power switches to get structure III (see Fig. 2).
2) Turn ON the power switches S_2, S_3, S_6, and S_7 in order to get the structure IV (see Fig. 2) while $\lambda_1 < 0$. Thus, variables evolve according to natural trajectory λ_4 (solid lines) with a radius established by the difference between the center of the circle corresponding to natural trajectory λ_4 and the point A. Once λ_1 becomes positive, then turn ON the corresponding power switches to get structure I (see Fig. 2).

It can be demonstrated that solution 2 allows a faster transient response to be obtained than does solution 1. Similar analysis can be applied for the different initial condition shown in Fig. 4.

IV. Control Law

The control law referred to as the NSS is discussed in this section. The NSS is defined based on the intersection of the different natural trajectories of the DAB converter and the target operating point.

In order to achieve the control objective, the SSs are arranged in the following sequence for one complete switching cycle: $\lambda_1 \rightarrow \lambda_2 \rightarrow \lambda_3 \rightarrow \lambda_4$ (16).

The behavior of the converter using the NSS can be synthesized in a simple conceptual definition. The objective of the NSS is to keep the operating point around the reference output voltage, and it must switch between positive and negative target inductor current. First, the operating point is directed toward the outside of the surface described by the intersection of the natural trajectories and the control objective until the boundary is reached. Thereafter, a change in the structure of the system is performed (u_1 and u_2 change) to force the operating point to follow the perimeter of the natural trajectory. During start-up operation, the converter initial condition is located at point A in Fig. 5(a), and the control forces the states $u_1 = 1$ and $u_2 = -1$ to move along the normalized inductor current axis until the surface λ_2 is reached at point B. When this switching surface is reached, the control law switch to state $u_1 = 1$ and $u_2 = 1$ up to arrive at point C is accomplished. Finally, state $u_1 = -1$ and $u_2 = 1$ is forced. This state is kept until the steady-state sequence is achieved. Once the steady-state surface is reached, the control law ensures that the operating point follows the reference of the output voltage. Both the output voltage and the transformer current are considered as varying references to establish a more accurate control law.

Fig. 5(b) shows the phase plane when maximum current limit mode is used. There are two imposed boundaries that prevent the natural trajectories from exceeding these limits, which are indicated in this figure as $\pm I_{\max}$. Using this mode, the maximum inductor current is limited to $|i_L| < I_{\max}$. The SSs are chosen in order to reach the steady-state condition after a few switching cycles, which are function of the value of the $I_{\max}$ imposed by the semiconductor devices and the transformer voltage balance. The control law makes the transitions to ensure that the sequence $\lambda_1 \rightarrow \lambda_2 \rightarrow \lambda_3 \rightarrow \lambda_4$ is met. When the maximum current limit mode is active the control law will need more switching actions to reach the target if a large output capacitor is used, but the

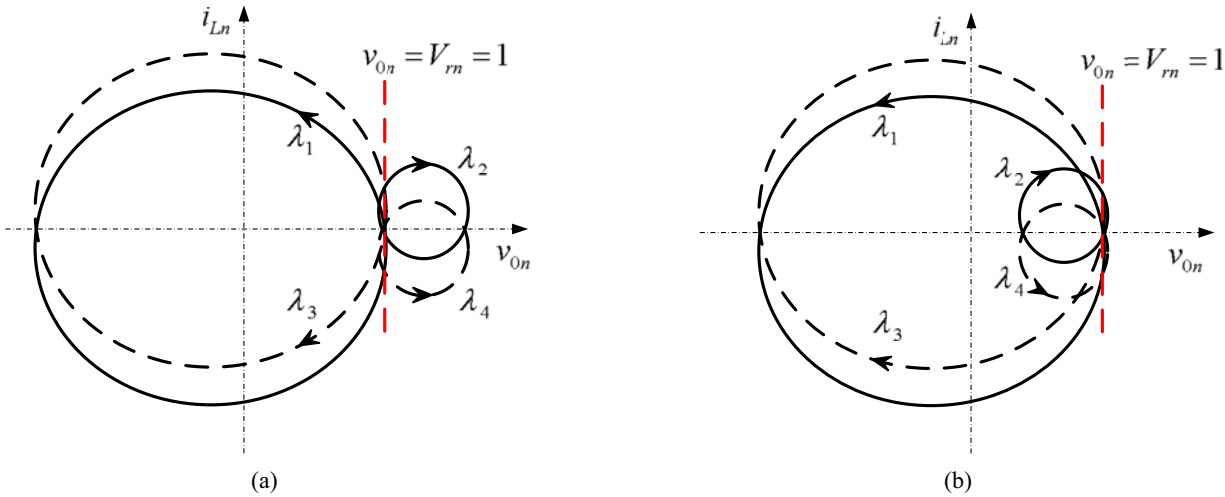

Fig. 3. Normalized natural trajectories for the DAB converter. (a) Buck mode. (b) Boost mode.

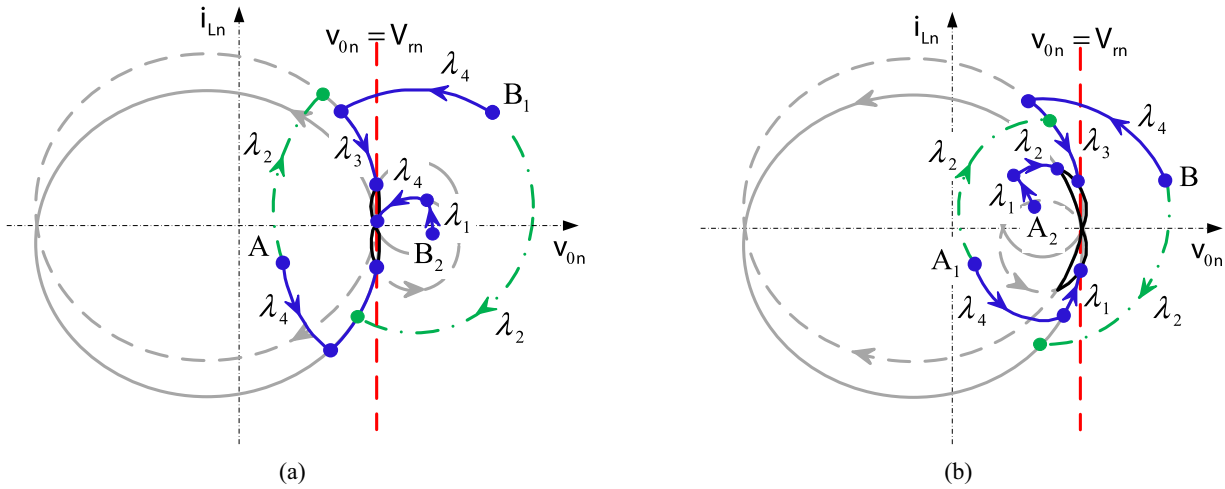

Fig. 4. Conceptual approach to the target for the DAB converter when initial output voltage is either lower (point A_x) or higher (point B_x) that reference: (a) Buck mode and (b) Boost mode.

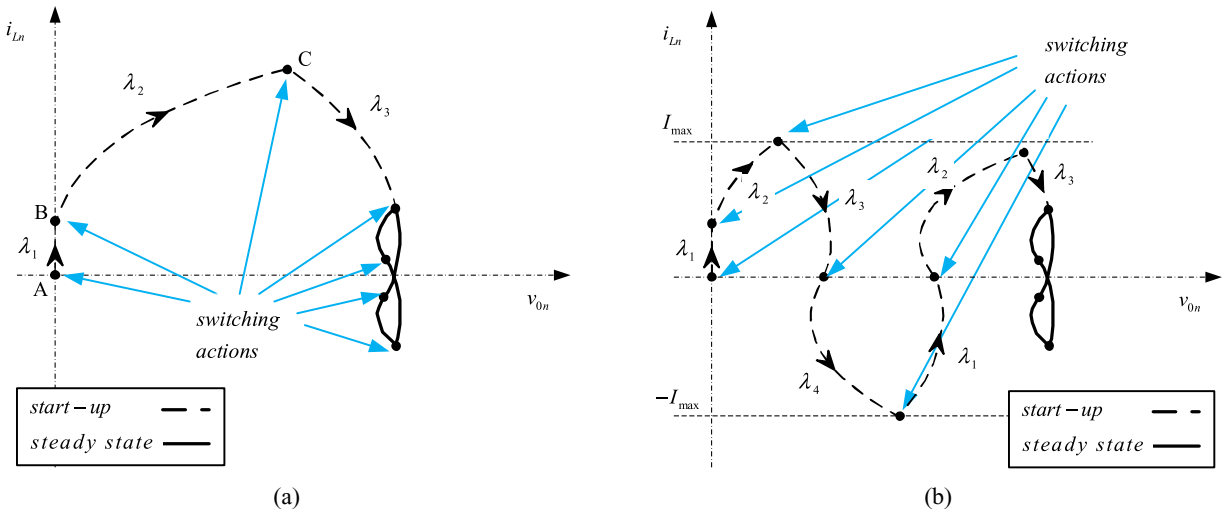

Fig. 5. Conceptual trajectories when the NSS is used during start-up: (a) without maximum current limit and (b) with maximum current limit.

trajectories selected allow the recovery time to be reduced. By using the control law with current boundary limit, a potential saturation of the transformer can be avoided by maintaining voltage balance. The physical transient limit of the system is given by the combination of V_{cc}, L, C, and loading condition. In particular, the relationship between the characteristic impedance Z_0 and the load resistor will determine if the transient can be solved in one of several switching cycles. For example, if the output capacitance is large and a heavy loading condition occurs, the converter might require several switching cycles to recharge this large capacitor.

It should be noted that the radius of the circles of the natural trajectories are function of the initial condition of the inductor current and output voltage, as can be deduced from (16). When maximum current limit mode is used, it is not necessary to recalculate the radius of the circles. Since the inductor current is known at all times, once it equals the current limit, a structure switching occurs in order to follow the sequence $\lambda_1 \rightarrow \lambda_2 \rightarrow \lambda_3 \rightarrow \lambda_4$.

The behavior of the converter during large signal transients is presented with the aid of Fig. 6. When the normalized output voltage of the converter is either lower or higher than the reference value, the control law directs the converter operating point toward the steady-state surface. For example, Fig. 6 shows two particular cases for buck [see Fig. 6(a)] and boost [see Fig. 6(b)] operating modes, which are described as follows: for buck mode, the normalized output voltage is lower than the reference value and the current i_{Ln} is positive, starting at point A_1. By analyzing the natural paths shown in Fig. 3, it can be deduced that only λ_2 and λ_3 can direct the operating point toward the surface corresponding to steady state. Since the initial point A_1 is inside the circle that determines the natural trajectory λ_3 ($\lambda_3|_A < 0$) the NSS first selects λ_2 ($\lambda_2|_A > 0$) until it reaches the surface λ_3, and then uses the last natural trajectory to reach the steady-state surface.

A similar analysis can be performed for the operating points A_2 in buck mode [see Fig. 6(a)], as well as points A_1 and A_2 in boost mode [see Fig. 6(b)]. As can be seen, all the trajectories depicted in Fig. 6 present the sequences to solve each particular transient case with fast response.

V. Steady-State Operation

In this section, DAB converter steady-state operation is explained and the expressions to operate the converter under constant switching frequency are derived. The control strategy is designed to operate the converter with constant frequency in steady-state operation. During transients, the frequency is modified to compensate and reach the target as soon as possible.

In order to establish the correspondence between phase plane and time domain the phase plane and waveforms of i_L and v_0 when the converter operates in steady state are shown in Fig. 7(a) and (b), respectively. In these figures, the different structures defined in Fig. 2 are indicated, which correspond to natural trajectories defined in (16) . Fig. 7(b) also shows transformer terminal voltages, v_{T1} and v_{T2}. From these figures, it can be observed that the output voltage is continuously changing around the reference output voltage following the sequence $\lambda_1 \rightarrow \lambda_2 \rightarrow \lambda_3 \rightarrow \lambda_4$, in a full switching period. It can be observed that in the intersection of the natural trajectories λ_1-λ_2 and λ_2-λ_3, the inductor current is equal to $i_{L\,A}$ and $i_{L\,B}$, respectively. Similarly, in the intersection between λ_3-λ_4 and λ_4-λ_1, the inductor current is equal to $-i_{L\,A}$ and $-i_{L\,B}$, respectively; due to the symmetry of the current waveform. These current values, which have been determined through previous research, are function of the operating point of the converter and the switching frequency [24], [25]. An important feature is that the average value of the inductor current in a switching period is equal to zero. This condition has to be fulfilled in order to avoid the saturation of the high-frequency transformer [12].

Fig. 8(a) and (b) shows the differences between the phase planes in steady state for buck and boost operation, according to the natural trajectories previously defined in Fig. 5.

A. Determination of $i_{Ln,\mathrm{target}}$.

The initial conditions of the inductor current can be determined in order to obtain the desired switching frequency in steady state. The value of $i_{Ln,\mathrm{target}}$ in (16) when the converter operates in steady state should be evaluated carefully. This value can vary significantly with the operating point and also according to the natural trajectory: λ_1, λ_2, λ_3, or λ_4. Thus, the initial condition can be evaluated using the steady-state current expression at the switching angles, $i_{L\,A}$ and $i_{L\,B}$ in Fig. 7, as (see [25])

$$i_{L\,A} = \frac{V_{cc}\,(2\delta - \pi + \pi d)}{2\omega^* L} \tag{18}$$

and

$$i_{L\,B} = \frac{V_{cc}\,(2d\delta + \pi - \pi d)}{2\omega^* L} \tag{19}$$

where $\omega^* = 2\pi f_s^*$, f_s^* is the desired switching frequency, $d = v_0/V_{cc}$ is the voltage conversion ratio, and δ is the phase-shift angle between v_{T1} and v_{T2} which can be determined as a function of the required output power in steady state, P_0, using the following expression [5]:

$$\delta = \frac{\pi}{2} - \frac{\sqrt{\left((V_{cc}d\pi)^2 - 4P_0 d\omega^* L\pi\right)}}{2V_{cc}d}. \tag{20}$$

By normalizing (18) and (19), the following expressions can be obtained:

$$i_{Ln\mathrm{A}} = \left(\frac{i_{L\,A}\,Z_0}{V_r}\right) \tag{21}$$

and

$$i_{Ln\mathrm{B}} = \left(\frac{i_{L\,B}\,Z_0}{V_r}\right). \tag{22}$$

To obtain constant switching frequency, the radius of the circles defined in (17) can be properly modified to match the points A and B in Fig. 7. Thus, by solving r from (17) so that the points A and B belong to the perimeter of the circle, the

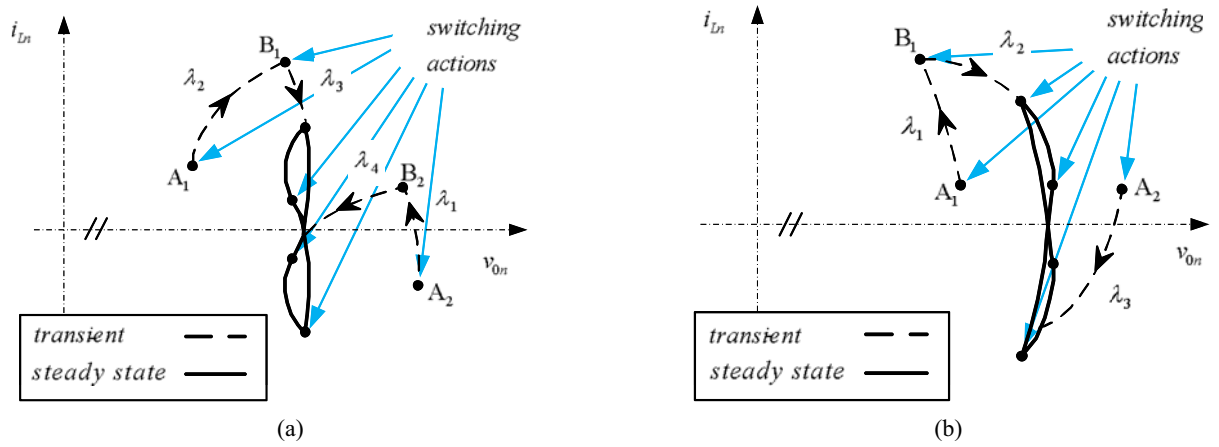

Fig. 6. Two particular normalized output voltage reference sudden change trajectories using the NSS: when the output voltage is lower than the reference voltage (point A_1) and when the output voltage is higher than the reference voltage (point A_2) for (a) buck mode; (b) boost mode.

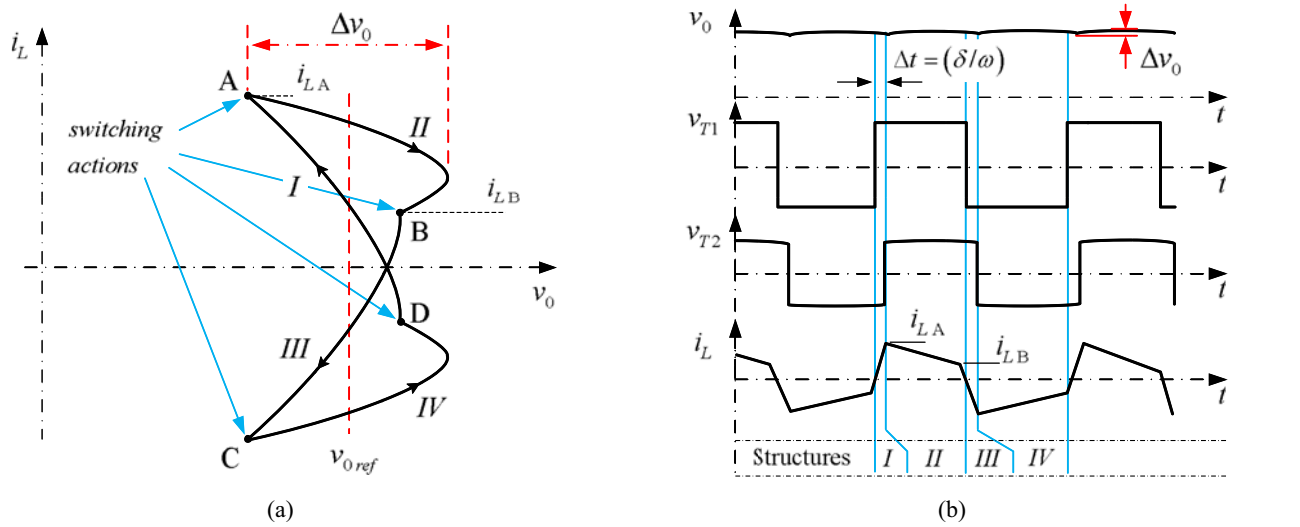

Fig. 7. Characteristic of steady state of the DAB converter operating in boost mode. (a) Phase plane of i_L versus v_0. (b) Steady-state waveforms corresponding to v_0, v_{T1}, v_{T2}, and i_L.

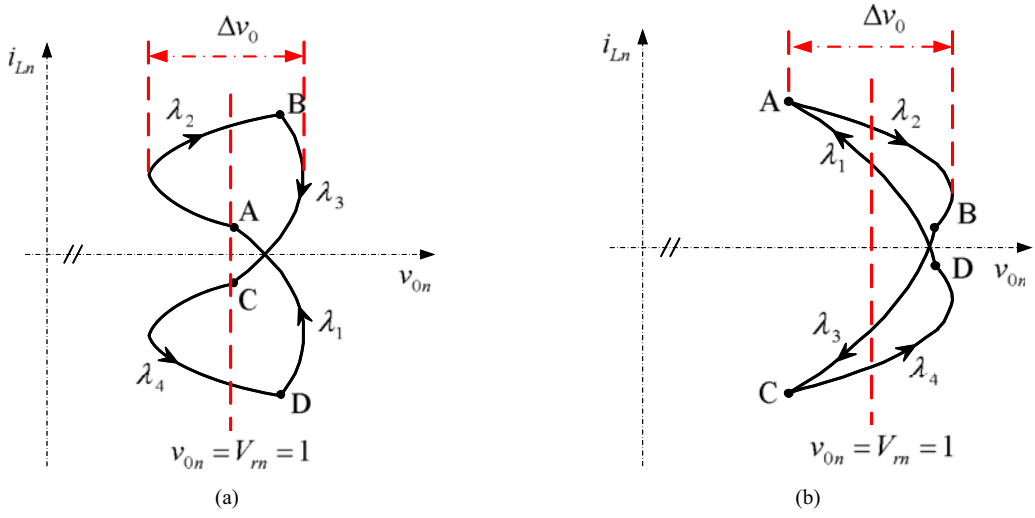

Fig. 8. NSS steady-state concept for the DAB Converter. (a) Buck mode. (b) Boost mode.

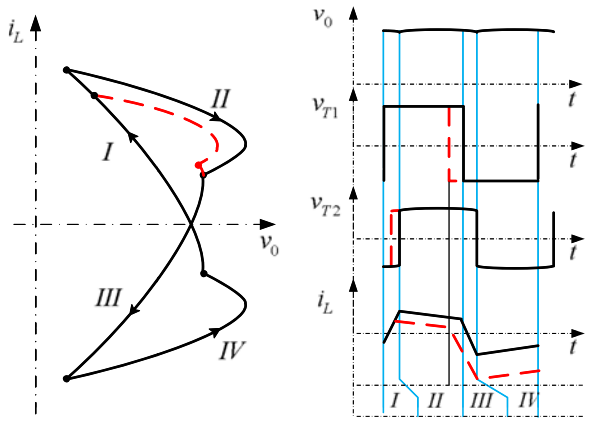

Fig. 9. Conceptual transformer voltage-second change with trajectory II.

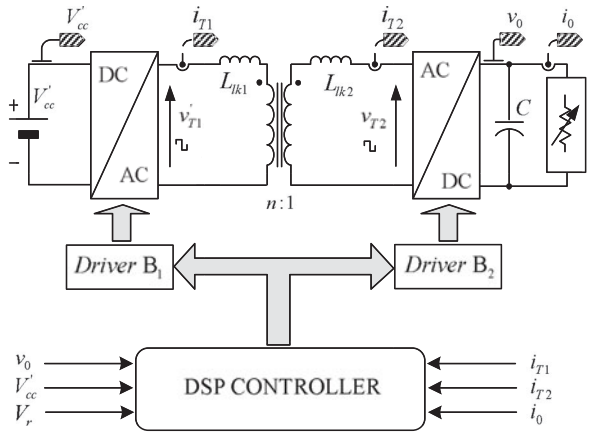

Fig. 10. Block diagram of the experimental setup.

following expression can be obtained:

$$r = \sqrt{x_2^2 - 2x_2x_0 + x_0^2 + y_2^2 - 2y_2y_0 + y_0^2} \tag{23}$$

where x_0 and y_0 are defined in (17), $x_2 = V_{rn}$, and $y_2 = -i_{LnB}$ for $\lambda_1(-\lambda_3)$ and $y_2 = i_{LnB}$ for $\lambda_2(-\lambda_4)$.

Finally, $i_{Ln,\text{target}}$ for each natural trajectory can be obtained by matching (23) with the radius expression defined in (17) yielding

$$i_{Ln,\text{target}}(\lambda_1) = -i_{0n} - \sqrt{\left(-V_{ccn}^2 - 2V_{ccn} - 1 + r_{\lambda_1}^2\right)} \tag{24}$$

$$i_{Ln,\text{target}}(\lambda_2) = -i_{0n} + \sqrt{\left(-V_{ccn}^2 + 2V_{ccn} - 1 + r_{\lambda_2}^2\right)} \tag{25}$$

$$i_{Ln,\text{target}}(\lambda_3) = -i_{Ln,\text{target}}(\lambda_1) \tag{26}$$

and

$$i_{Ln,\text{target}}(\lambda_4) = -i_{Ln,\text{target}}(\lambda_2) \tag{27}$$

where

$$r_{\lambda_1} = \left(1 + 2V_{ccn} + V_{ccn}^2 + (i_{LnB} - i_{on})^2\right) \tag{28}$$

and

$$r_{\lambda_2} = \left(1 - 2V_{ccn} + V_{ccn}^2 + (i_{LnB} - i_{on})^2\right). \tag{29}$$

B. Transformer Volt-Second Balance

The mechanism to prevent saturation in steady-state operation is achieved by means of controlling trajectories II and IV. Fig. 9 shows conceptually a modification of trajectory II to modify the current set-point when a dc component is present. Dashed lines in the time-domain plot display the effect on the duty cycle of the primary and secondary voltages that result from changing the equivalent radius of each natural trajectory in the geometrical domain. Current sensors in both the primary and secondary are required, as indicated in the conceptual system diagram in Fig. 10. Alternatively, for low power applications, a series capacitor that can be included, this should be able to withstand the ripple current.

TABLE I
EXPERIMENTAL PROTOTYPE CHARACTERISTICS

Maximum output power ($P_{0\max}$)	625 W
Switching frequency (f_s)	22 kHz
Output voltage (V_0)	50 - 60 V
Input voltage (V_{cc})	150 V
Transformer turns ratio (n)	1/5
Voltage conversion ratio $d = V_0/(nV_{cc})$	1.6 - 2
Total inductance (L)	15 μH
Output capacitor (C)	20 μF
Maximum inductor current	30 A

VI. SIMULATION AND EXPERIMENTAL RESULTS

Simulation and experimental results of a DAB converter are presented in this section to verify the behavior of the NSS, when the converter is operated in boost mode. Boost mode corresponds to values of the voltage conversion ratio higher than 1, where the voltage conversion ratio is defined as the relationship between the input voltage and output voltage affected by the transformer turns ratio, as it is shown in Table I [6]. Table I presents the converter specifications and Fig. 10 shows a block diagram of the experimental setup. The natural SS control laws were implemented using a TMS320F2812 fixed-point DSP.

Hall-effect sensors are used in the implementation to measure current waveforms and voltage signals. Alternatively, in order to reduce cost, shunt resistors can be used on the converter side that shares power ground with the DSP controller ground. Measuring multiple inputs can be achieved without increasing the cost of the system since low cost DSPs or microcontrollers have 8 or 16 analog inputs. It should be noted that the sensors selected to implement this advanced control technique are also used to protect the converter (typical input/output overcurrent and input/output overvoltage protections). Therefore, many traditional control strategies would also require a similar number of sensors.

When the converter is not operating, the output voltage is equal to zero. Therefore, at start-up it is necessary to increase the output voltage to 50 V in a few switching actions. The obtained start-up transient is shown in Fig. 11(a). During this transient, the control law determines the sequence explained in Section IV [see Fig. 5(b)] from time zero until steady state

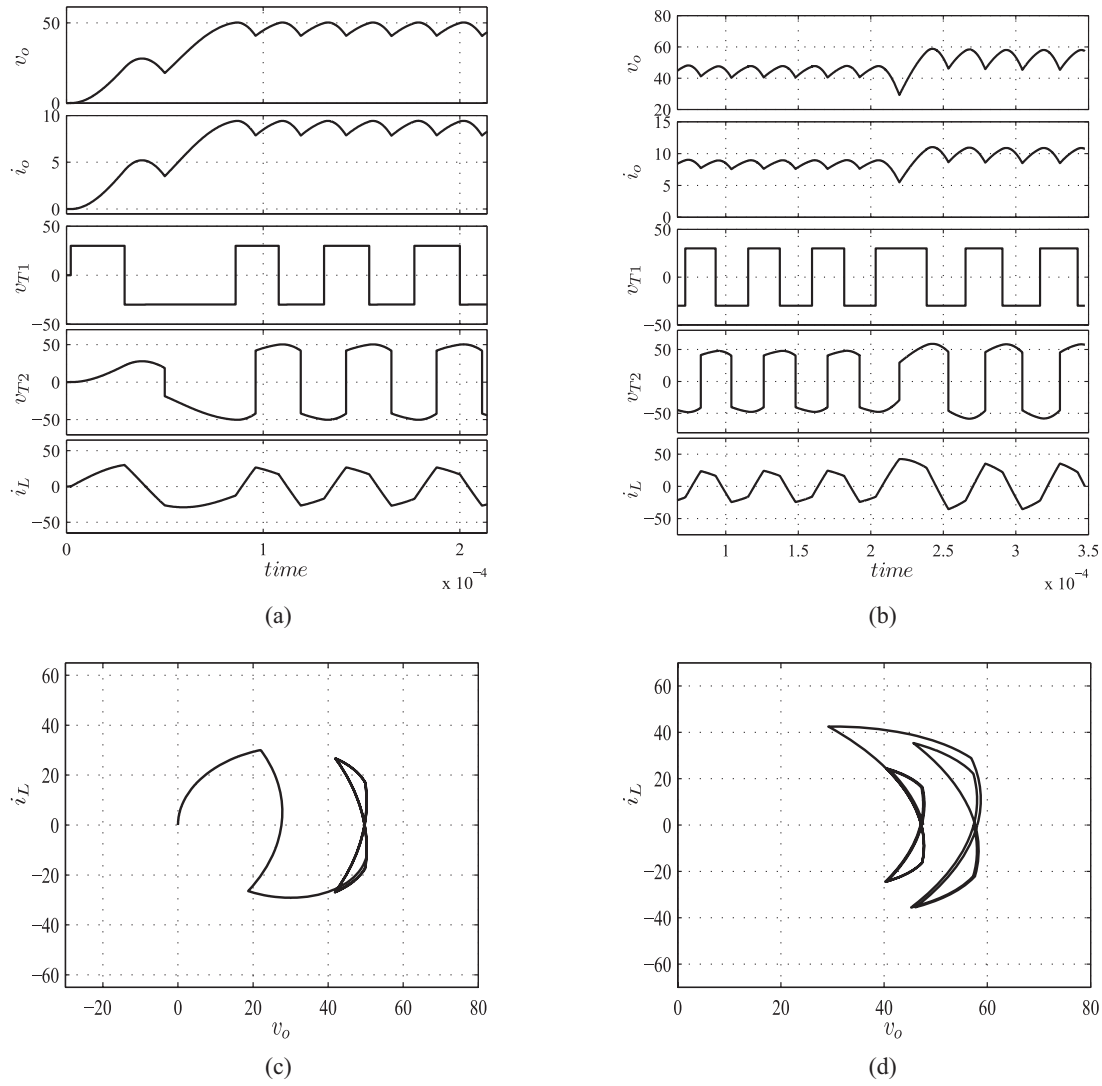

Fig. 11. Simulation results of the DAB converter using the NSS. (a) Start-up transient and (c) start-up phase-plane. (b) Sudden output voltage reference change and (d) output voltage reference change phase-plane.

is reached. Hence, the response has no overshoot and steady state is reached in a few switching actions. Fig. 11(c) shows the normalized state plane trajectories during start-up as described before.

Fig. 11(b) shows the response of the converter when the reference changes from 30 to 40 V. The converter reverts to steady state in only one switching action. Fig. 11(d) depicts the normalized state plane trajectories during a sudden change of reference.

As can be seen in the experimental capture of Fig. 12(a), during start-up the voltage reference is achieved in five switching actions with no overshoot, as predicted by the theory presented in this paper.

Fig. 12(b) shows the dynamic response of the converter for sudden changes of reference, reaching the target operating point in one switching action. It is worth noting that the dynamic behavior using a resistive load is comparable to the constant current load case. In order to provide further insight into the evolution of the state trajectories, the experimental state plane trajectories during start-up and reference-change transients are presented in Fig. 13.

Fig. 14 shows the simulated dynamic response of the converter for sudden resistive load change [from 9 to 12.5 A in Fig. 14(a) and from 12.5 to 9 A in Fig. 14(b)], reaching the target operating point in one switching action. Fig. 15(a) and (b) shows the experimental dynamic responses of the discussed load change transients.

In all cases, the experimental results are in close agreement with the simulation results. The ringing observed in experimental waveforms is due to small parasitic components in the PCB and transformer (e.g., interwinding capacitance). Since the oscillations occur at high frequencies (MHz), it is not necessary to include them in the NSS derivation.

The converter operates in ZVS operation in steady state under a wide range of output power conditions, due to the conversion ratio and output power adopted [7], [24]. Since the proposal considers a traditional modulation sequence, opportunities for

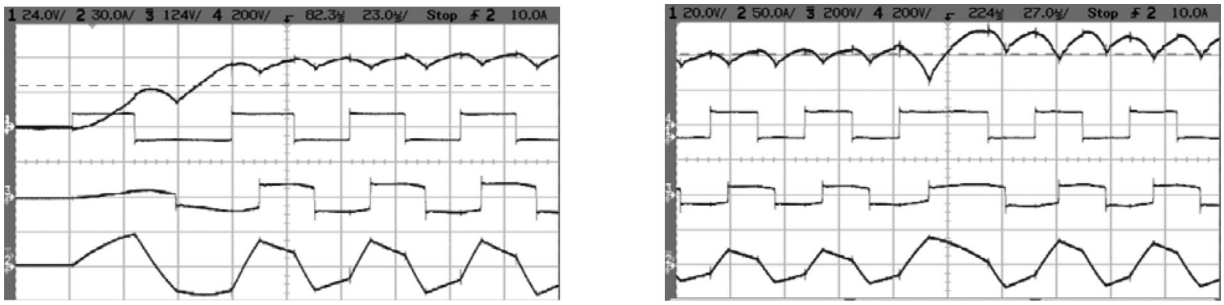

(a) (b)

Fig. 12. Experimental results of the DAB converter using the NSS for (a) start-up transient and (b) sudden output voltage reference. Output voltage (Ch1), inductor current (Ch2), secondary voltage (Ch3), and primary voltage (Ch4).

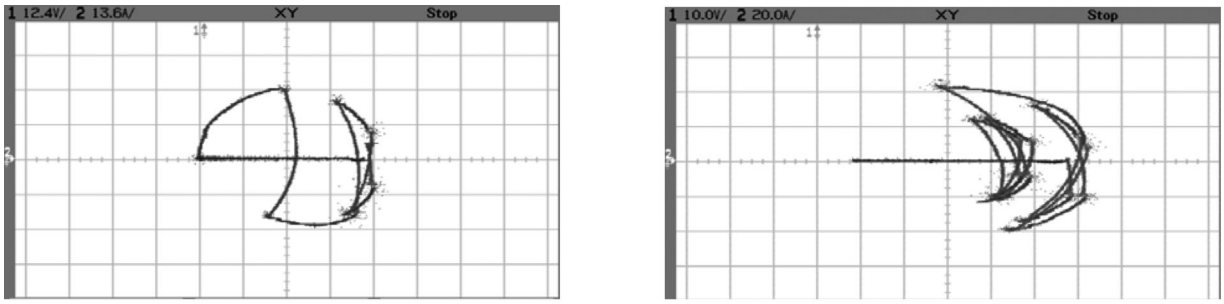

(a) (b)

Fig. 13. Experimental phase planes of the DAB converter using the NSS for (a) start-up and (b) sudden output voltage reference change: output voltage (Ch1) and inductor current (Ch2).

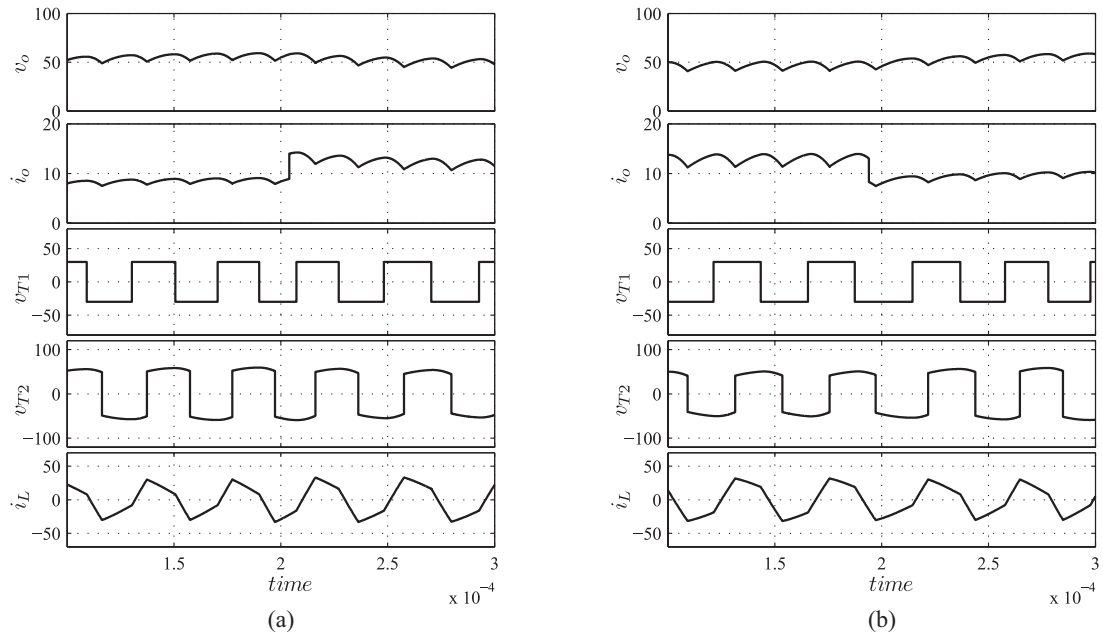

(a) (b)

Fig. 14. Load change simulation results for the DAB Converter using the NSS: (a) step-up load transient and (b) step-down load transient.

modified modulations are open for investigation beyond the regulations limits described. Therefore, switching losses can be reduced by developing new switching sequences in steady state. This subject is beyond the scope of this paper and will be investigated in the future. Regarding power losses during transient operation (transient analysis is the main focus of the paper), the idea of minimizing the number of switching actions contributes to the reduction of switching losses. During transient,

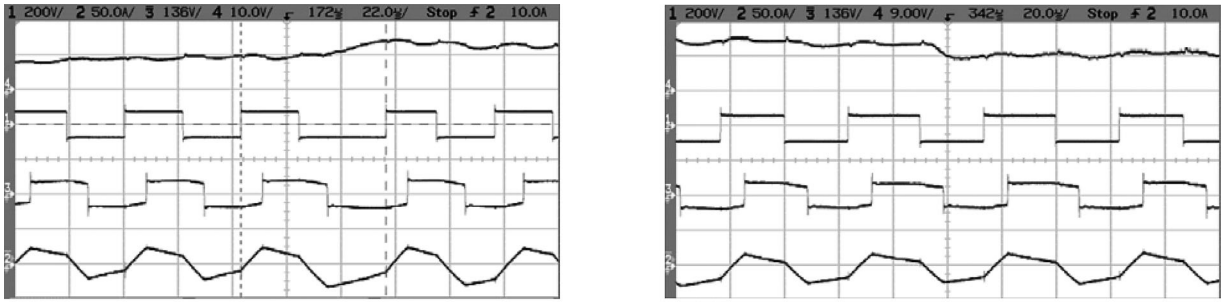

(a) (b)

Fig. 15. Load change experimental results for the DAB Converter using the NSS: primary voltage (Ch1), inductor current (Ch2), secondary voltage (Ch3), and output current (Ch4).

it should be noted that one or more switching action could occur in hard switching, like in any other control strategy for DAB. The contribution to losses is almost negligible due to the short duration.

VII. Conclusion

A curved switching surface for control of DAB converters was presented in this paper. The natural trajectories of the system and the NSS were derived in the normalized domain to provide generality to the analysis. Under the NSS control scheme, the converter showed excellent dynamic behavior, with no overshoot and fast transient response for start-up and load disturbances, achieving steady state in a few switching actions. In addition to the enhanced dynamic response, fixed-frequency operation was realized by employing discrete reference changes. A normalized analysis framework was presented and illustrated with a 625 W, 150 V /50 V example that was simulated and verified with experimental results. The implemented prototype was employed to test the case example, confirming the enhanced characteristics of the proposed technique.

References

[1] P. Nema, R. K. Nema, and S. Rangnekara, "A current and future state of art development of hybrid energy system using wind and PV-solar: A review," *Elsevier Renewable Sustain. Energy*, vol. 13, no. 8, pp. 2096–2103, Oct. 2009.

[2] N. Liqin, D. J. Patterson, and J. L. Hudgins, "High power current sensorless bidirectional 16–phase interleaved dc–dc converter for hybrid vehicle application," *IEEE Trans. Power Electron.*, vol. 27, no. 3, pp. 1141–1151, Mar. 2012.

[3] F. Krismer and J. W. Kolar, "Accurate power loss model derivation of a high-current dual active bridge converter for an automotive application," *IEEE Trans. Ind. Electron.*, vol. 57, no. 3, pp. 881–891, Mar. 2010.

[4] Z. Wang and H. Li, "A soft switching three-phase current-fed bidirectional dc–dc converter with high efficiency over a wide input voltage range," *IEEE Trans. Power Electron.*, vol. 27, no. 2, pp. 669–684, Feb. 2012.

[5] G. G. Oggier, G. O. García, and A. R. Oliva, "Modulation strategy to operate the dual active bridge dc–dc converter under soft-switching in the whole operating range," *IEEE Trans. Power Electron.*, vol. 26, no. 4, pp. 1228–1236, Apr. 2011.

[6] M. H. Kheraluwala, R. W. Gascoigne, D. M. Divan, and E. D. Baumann, "Performance characterization of a high-power dual active bridge dc-to-dc converter," *IEEE Trans. Ind. Appl.*, vol. 28, no. 6, pp. 1294–1301, Nov./Dec. 1992.

[7] F. Krismer and J. W. Kolar, "Efficiency-optimized high-current dual active bridge converter for automotive applications," *IEEE Trans. Ind. Electron.*, vol. 59, no. 7, pp. 2745–2760, Jul. 2012.

[8] F. Krismer and J. W. Kolar, "Closed form solution for minimum conduction loss modulation of DAB converters," *IEEE Trans. Power Electron.*, vol. 27, no. 1, pp. 174–188, Jan. 2012.

[9] N. M. L. Tan, T. Abe, and H. Akagi, "Design and performance of a bidirectional isolated dc–dc converter for a battery energy storage system," *IEEE Trans. Power Electron.*, vol. 27, no. 3, pp. 1237–1248, Mar. 2012.

[10] N. M. L. Tan, S. Inoue, A. Kobayashi, and H. Akagi, "Voltage balancing of a 320-V, 12-F electric double-layer capacitor bank combined with a 10-kW bidirectional isolated dc–dc converter," *IEEE Trans. Power Electron.*, vol. 23, no. 6, pp. 2755–2765, Apr. 2008.

[11] M. B. Camara, H. Gualous, F. Gustin, A. Berthon, and B. Dakyo, "DC/DC converter design for supercapacitor and battery power management in hybrid vehicle applications—Polynomial control strategy," *IEEE Trans. Ind. Electron.*, vol. 57, no. 2, pp. 587–597, Apr. 2010.

[12] R. W. Erickson and D. Maksimovic, *Fundamentals of Power Electronics*, 2nd ed. Boston, MA, USA: Kluwer, 2001, ch. 6.

[13] H. Qin and J. W. Kimball, "Generalized average modeling of dual active bridge DC–DC converter," *IEEE Trans. Power Electron.*, vol. 27, no. 4, pp. 2078–2084, Apr. 2012.

[14] F. Z. Peng, H. Li, G. Su, and J. S. Lawler, "A new ZVS bidirectional dc–dc converter for fuel cell and battery application," *IEEE Trans. Power Electron.*, vol. 19, no. 1, pp. 54–65, Jun. 2004.

[15] F. Krismer and J. W. Kolar, "Accurate small-signal model for the digital control of an automotive bidirectional dual active bridge," *IEEE Trans. Power Electron.*, vol. 24, no. 12, pp. 2756–2768, Dec. 2009.

[16] A. R. Oliva, S. S. Ang, and G. E. Bortolotto, "Digital control of a voltage-mode synchronous buck converter," *IEEE Trans. Power Electron.*, vol. 21, no. 1, pp. 175–163, Dec. 2006.

[17] D. Segaran, D. G. Holmes, and B. P. McGrath, "Enhanced load step response for a bidirectional dc–dc converter," *IEEE Trans. Power Electron.*, vol. 28, no. 1, pp. 371–379, Jan. 2013.

[18] D. D. M. Cardozo, J. C. Balda, D. Trowler, and H. A. Mantooth, "Novel nonlinear control of dual active bridge using simplified converter model," in *Proc. IEEE Appl. Power Electron. Conf.*, Feb. 2010, pp. 321–327.

[19] J. M. Galvez, M. Ordonez, F. Luchino, and J. E. Quaicoe, "Improvements in boundary control of boost converters using the natural switching surface," *IEEE Trans. Power Electron.*, vol. 26, no. 11, pp. 3367–3376, Nov. 2011.

[20] M. Ordonez, M. T. Iqbal, and J. E. Quaicoe, "Selection of a curved switching surface for buck converters," *IEEE Trans. Power Electron.*, vol. 21, no. 4, pp. 1148–1153, Jul. 2006.

[21] M. Ordonez, J. E. Quaicoe, and M. T. Iqbal, "Advanced boundary control of inverters using the natural switching surface: Normalized geometrical derivation," *IEEE Trans. Power Electron.*, vol. 23, no. 6, pp. 2915–2930, Nov. 2008.

[22] W. Feng, F. C. Lee, and P. Mattavelli, "Simplified optimal trajectory control (SOTC) for LLC resonant converters," *IEEE Trans. Power Electron.*, vol. 28, no. 5, pp. 2415–2426, May 2013.

[23] M. Greuel, R. Muyshondt, and P. T. Krein, "Design approaches to boundary controllers," in *Proc. IEEE Power Electron. Spec. Conf.*, Jun. 1997, pp. 22–27.

[24] R. W. De Doncker, D. M. Divan, and M. H. Kheraluwala, "A three phase soft-switched high-power-density dc/dc converter for high-power applications," *IEEE Trans. Ind. Appl.*, vol. 27, no. 1, pp. 63–73, Jan./Feb. 1991.

[25] G. G. Oggier, G. O. García, and A. R. Oliva, "Switching control strategy to minimize dual active bridge converter losses," *IEEE Trans. Power Electron.*, vol. 24, no. 7, pp. 1826–1838, Jul. 2009.

Germán G. Oggier (M'10) was born in Córdoba, Argentina. He received the Electr. Eng. degree, in 2003, and the M.Sc. degree in electrical engineering, in 2006, both from the Universidad Nacional de Río Cuarto, Río Cuarto, Argentina, and the Doctorate degree in control systems from the Universidad Nacional del Sur, Buenos Aires Province, Argentina, in 2009.

During 2011–2012, he was a Postdoctoral Fellow with Simon Fraser University, Metro Vancouver, BC, Canada. The postdoctoral research activities were in the area of boundary control of power converters. He is currently a Lecturer in the Grupo de Electrónica Aplicada, Universidad Nacional de Río Cuarto. He is also a Researcher with the Consejo Nacional de Investigaciones Científicas y Técnicas, Buenos Aires, Argentina. His current research interests include power electronics, electric vehicles, and renewable energy conversion.

Martin Ordonez (S'02–M'09) was born in Neuquen, Argentina. He received the Ing. degree in electronics engineering from the National Technological University, Argentina, in 2003, and the M.Eng. and Ph.D. degrees in electrical engineering from the Memorial University of Newfoundland, St. John's, NL, Canada, in 2006 and 2009, respectively.

He is currently an Assistant Professor with the Department of Electrical and Computer Engineering, The University of British Columbia (UBC), Vancouver, BC, Canada. He is also an Adjunct Professor with Simon Fraser University (SFU), Burnaby, BC and the Memorial University of Newfoundland (MUN). His industrial experience in power conversion includes research and development at Xantrex Technology, Inc./Elgar Electronics Corporation (now AMETEK Programmable Power), Deep-Ing Electronica de Potencia, and TRV Dispositivos, where he developed high-density dc–dc power converters, UPS inverters, and digital controllers. He has an active research program in power conversion for renewable energy systems and has developed partnerships with various companies in the sector. With the support of industrial funds and the Natural Sciences and Engineering Research Council (NSERC), he contributed more than 50 publications and R&D reports in the power area.

Dr. Ordonez received the David Dunsiger Award for excellence in the Faculty of Engineering and Applied Science (2009) and the Chancelloros Graduate Award/Birks Graduate Medal (2006). He was a Fellow of the School of Graduate, Memorial University.

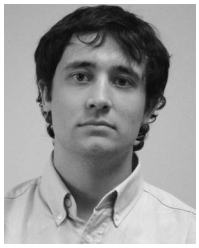

Juan M. Galvez (S'10) was born in Cordoba, Argentina. He received the Ing. degree in electronics engineering from National Technological University, Argentina, in 2010, and the M.A.Sc. degree from Simon Fraser University (SFU), Burnaby, BC, Canada, in 2012. He is currently working toward the Ph.D. degree at the University of British Columbia (UBC), Vancouver, BC.

His current research interests include dc/dc power converters, power factor correctors, and nonlinear control for renewable power applications.

Mr. Galvez received the National Academy of Engineering Award (2010) for undergraduate studies, Argentina, and the C.D. Nelson Memorial Graduate Scholarship (2012–2015) from the Dean of Graduate Studies, SFU, and the Four-Year-fellowship (2013–2016) from the Department of Electrical and Computer Engineering, UBC. He was also recognized in 2006 with a research scholarship by the Science and Technology Office, National Technological University, Argentina.

Federico Luchino (S'10) received the Ing. degree in electronics engineering from National Technological University, Buenos Aires, Argentina, in 2005, and the M.A.Sc. degree from Simon Fraser University, Burnaby, BC, Canada, in 2012.

His professional experience includes development of electronic hardware and firmware for several companies in Argentina and Spain. He was awarded with a Scholarship from the School of Graduate Studies, Memorial University (2010–2011). He was also recognized for six consecutive years (2000–2005) with a research scholarship by the Science and Technology Office, National Technological University, Argentina.